Thickness dependent transport properties of compressively strained $La_{0.88}Sr_{0.12}MnO_3$ ultrathin films

Ravikant Prasad,[1] H. K. Singh,[1,a)] M. P. Singh,[2,b)] W. Prellier,[2] P. K. Siwach,[3] and Amarjeet Kaur[4]
[1]*National Physical Laboratory, Dr. K. S. Krishnan Road, New Delhi 110012, India*
[2]*Laboratoire CRISMAT, ENSICAEN, UMR 6508, F-14050 Caen Cedex, France*
[3]*UGC-DAE, Consortium for Scientific Research, Khandwa Road, Indore 452001, India*
[4]*Department of Physics and Astrophysics, University of Delhi, Delhi 110007, India*

(Received 10 November 2007; accepted 22 January 2008; published online 18 April 2008)

Thickness dependent magnetic and transport properties of compressively strained $La_{0.88}Sr_{0.12}MnO_3$ thin films grown on single crystalline $SrTiO_3$ (100) substrates have been studied. All films exhibit a large enhancement of ~ 130 K in T_C/T_{IM} as compared to that of the bulk target ($T_C \sim 175$ K). This has been explained in terms of suppression of the cooperative *Jahn–Teller* distortion due to in-plane compressive strain. The T_C/T_{IM} of the 5 nm film is 315 K/318 K and slightly increases for film thicknesses ≤ 25 nm. At higher film thicknesses, ~ 60 nm, the T_C/T_{IM} starts decreasing. At $T > T_{IM}$, the electrical transport is due to thermally activated hopping of small polarons. The activation energy is found to be sensitive to film thickness and shows a minimum at around $L \sim 15–25$ nm, which corresponds to the maximum of T_C/T_{IM}. All films possess large magnetoresistances (MRs) in the vicinity of room temperature. Low as well as high field MRs are observed to nearly double as the film thickness increases from 5 nm (MR $\sim 28\%/3$ T) to 60 nm (MR% $\sim 50\%/3$ T). Thicker films ($L \geq 25$ nm) are found to exhibit sufficiently large temperature coefficients of resistivities, $\sim 4\%–5\%/\mathrm{K}$, which could be suitable for bolometric applications.
© *2008 American Institute of Physics*. [DOI: 10.1063/1.2902927]

I. INTRODUCTION

Doped rare earth perovskite manganites, which are represented by $RE_{1-x}AE_xMnO_3$ (RE=La, Nd, Pr, etc., and AE =Ca, Sr, Ba, Pb, etc.), exhibit strong sensitivity to the magnetic field resulting in the colossal magnetoresistance (CMR) effect that is generally observed in the doping range $x \sim 0.2–0.4$.[1–7] The electronic phase diagram of this strongly correlated class of materials is very rich. Manganites, depending on the value of x and temperature, exhibit a variety of ordering and transitions, such as paramagnetic (PM) to ferromagnetic (FM) transition, insulator to metal (IM) transition, charge-orbital ordering (COO), and antiferromagnetic (AFM) ordering, which often result in phase coexistence, i.e., phase separation.[6] The CMR effect is found in the vicinity of the FM-PM transition point (Curie temperature T_C) that lies in the proximity of the IM transition temperature (T_{IM}).[1–3] In polycrystalline and single crystal materials, the CMR effect primarily depends on x.[4–7] The FM double exchange (FM-DE) is invoked to explain the magnetic and transport properties of the manganites in the CMR regime.[1–7] However, it has now been accepted in general that FM-DE, due to the restricted validity in the vicinity of T_C/T_{IM}, is not sufficient to explain the various physical properties of manganites. Consequently, other interactions, which compete with the FM-DE mechanism, such as electron-lattice coupling, are also known to play a key role, as demonstrated by the oxygen isotope effect.[8–10] One particular mechanism for this coupling is the Jahn–Teller (JT) distortion/effect of the MnO_6 octahedrons, which lifts the degeneracy of the Mn e_g levels in a cubic environment by biaxial distortion.[8] Depending on the value of x, other intrinsic phenomena, such as COO and AFM ordering, are also found to play an important role in determining the overall landscape of manganites.[4–7]

The CMR effect in manganite thin films can be tailored by biaxial strain. In epitaxial thin films grown on perovskite substrates, the biaxial strain that can be induced by lattice mismatch with the underlying substrate, film thickness, oxygen content, etc., provides an additional degree of freedom and, hence, influences the magnetic and transport properties.[11–17] In the case of a film grown on a given substrate, the strain mainly depends on the thickness. Beyond a critical film thickness, the strain is gradually relaxed and this aspect also has decisive influence on magnetic and transport properties, such as magnetization, T_C, and T_{IM}.[11–14,16,17] The effect of biaxial distortion induced by substrate strain is expected to be fundamentally different from the effect of bulk (compressive) strain driving the lattice toward cubic symmetry, hence, strongly affecting the subtle interplay between spin, charge, structural, and orbital degrees of freedom. Therefore, the clarification of the detailed role of biaxial strain is essential and has been recently addressed in several experimental studies.[18–35] Strain has also been found to significantly affect the conduction noise properties.[36]

Among the manganites, the divalent-doped $La_{1-x}Sr_xMnO_3$ ($0.1 < x < 0.5$), because of its large one electron bandwidth, is of great interest. It undergoes simultaneous PM-FM and IM transitions at different temperatures

[a)]Author to whom correspondence should be addressed. Electronic mail: hks65@mail.nplindia.ernet.in.
[b)]Present address: Département de Physique and RQMP, Université de Sherbrooke, Sherbrooke-J1K 2R1, Canada.

 © 2008 American Institute of Physics

Downloaded 29 Apr 2009 to 202.141.140.34. Redistribution subject to AIP license or copyright; see http://jap.aip.org/jap/copyright.jsp

depending on the value of x.[37] Several interesting features have been observed in this system in the composition range of $0.1<x<0.18$, e.g., the observation of structural phase transitions accompanying various magnetic phase transitions at temperatures below 300 K.[38] At lower values of x, the MnO_6 octahedrons are heavily distorted in the in-plane directions (elongated in the in-plane direction and, hence, compressed in the out-of-plane direction), and consequently, the JT effect dominates the FM-DE.[8,9,37] A JT distortion of the MnO_6 octahedron can lead to the trapping of the charge carriers into a polaronic state, influencing the transport properties in the high temperature regime. However, the MnO_6 octahedron can be manipulated under the influence of in-plane compressive strain. Extensive studies have been carried out on thin films of $La_{1-x}Sr_xMnO_3$.[39–52] The effects of strain-film-thickness-induced modifications in various physical properties, such as magnetotransport and magnetic properties,[44–57] magnetic anisotropy,[39,40] optical properties,[40,50] and conduction noise,[38] have been investigated. However, nearly all of the studies related to the effect of strain have focused on $La_{1-x}Sr_xMnO_3$ with a doping level of $x\sim 0.3$ in which the one electron (e_g) bandwidth is large. Very little attention has been paid to strain-induced modifications in the transport properties in lightly doped $La_{1-x}Sr_xMnO_3$ ($x<0.15$).

Lightly doped $La_{1-x}Sr_xMnO_3$ exhibits a number of intriguing phenomena that arise due to the strong interplay between various degrees of freedom, such as spin, lattice, charge, and orbital degrees of freedom.[38,53] At smaller values of x, the JT effect dominates the FM-DE, resulting in lower T_C values. In the underdoped regime, $T_C \leq 200$ K;[53] hence, it is possible to investigate the resistivity in the PM regime over a broad temperature range. However, the most important attribute of the lightly doped $La_{1-x}Sr_xMnO_3$ is that the pressure derivative of T_C, i.e., dT_C/dP, peaks at around $x\sim 0.11-12$ and is expected to be the largest among the manganese perovskites.[54] Razavi *et al.*[15,55] showed that there is a possible pressure-induced polaronic to itinerant electronic transition in $La_{1-x}Sr_xMnO_3$ for $x=0.12$ and 0.15 that decreases upon application of pressure. Chen *et al.*[56,57] studied $x=0.10$ compounds in thin film form. They have observed near doubling of T_C/T_{IM} of $La_{0.9}Sr_{0.1}MnO_3$ ultrathin films.[57] This has been attributed to the in-plane epitaxially compressive strain effect, which suppresses the strong JT distortion.[57] However, possible causes of such large T_{IM}/T_C enhancement cannot be the hopping integral alone; hence, orbital degree of freedom and multiphase coexistence may play an important role. Prasad *et al.*[58] observed a similar T_C/T_{IM} enhancement and significant magnetoresistance (MR) and temperature coefficient of resistivity (TCR) for $La_{0.88}Sr_{0.12}MnO_3$ thin films deposited by on-axis dc magnetron sputtering on $SrTiO_3$ (STO) and $LaAlO_3$ (LAO) substrates. In view of the encouraging results for compressively strained thin films of lightly doped manganites such as $La_{1-x}Sr_xMnO_3$ ($x\sim 0.10-0.12$), a more comprehensive investigation of the evolution of magnetic and magnetotransport properties with film thickness is required. The variation in film thickness beyond a critical value leads to the relaxation of the strain, resulting in the formation of a variety of lattice defects, such as vacancies, stacking faults, and dislocation networks,[15–37] which has a profound effect on the magnetotransport properties. In this study, we report the influence of film thickness on the magnetoelectrical and magnetotransport properties of compressively strained $La_{0.88}Sr_{0.12}MnO_3$ thin films on STO single crystal substrates. The film thickness is varied from 5 to 60 nm.

II. EXPERIMENTAL DETAILS

The sputtering target was prepared from $La_{0.88}Sr_{0.12}MnO_3$ (LS8812) powders synthesized by a wet chemical route. High purity (>99.9%) metal nitrates, viz., $La(NO_3)_3\cdot 6H_2O$, $Sr(NO_3)_2$, and $Mn(NO_3)_2\cdot 4H_2O$, were dissolved in 150 ml of de-ionized water and an equal volume of ethylene glycol was added. The mixture was heated at 100 °C with constant stirring until a resin was formed. This resin was decomposed at 300 °C and finely crushed. The resultant powder was vigorously mixed and then heated for 12 h at 700 °C to get a highly homogenized LS8812 powder for the target. The detailed wet chemical process is given elsewhere.[59] The LS8812 powder was thoroughly mixed and then pressed to form the target pellet (⌀=2 in.) with a thickness of 3 mm. The final sintering of the target (⌀=2 in.) was carried out at 1300 °C for about 12 h. For various analytical studies, a second pellet (⌀=1 in.) was prepared along with the target. The powder x-ray diffraction (XRD) reveals that the LS8812 target is single phase and has a distorted perovskite structure with the *Pbnm* space group. The unit cell lattice parameters were found to be $a\sim 5.56$ Å ($a/\sqrt{2}\sim 3.93$ Å), $b\sim 5.54$ Å ($b/\sqrt{2}\sim 3.92$ Å), and $c\sim 7.74$ Å ($c/2\sim 3.87$ Å). This gives the average in-plane lattice parameter $a_{av}=(a_b+b_b)/2\sim 3.925$ Å. The average grain size was determined from surface morphological investigations by SEM to be ~500 nm. The bulk target has a FM $T_C\sim 175$ K and undergoes an IM transition at $T_{IM}\sim 145$ K. It exhibits a MR typical of polycrystalline manganites with submicron grain size, viz., the low field MR ($H\sim 3$ kOe) increases with decreasing temperature. To simulate the in-plane pressure effect by a compressive strain, we have chosen a STO (100) substrate that has the lattice parameter $a_S=3.905$ Å, which is smaller than the average in-plane lattice parameter of the bulk target ($a_t=a_{av}=3.925$ Å), and, hence, is suitable for inducing large in-plane compression. The average lattice mismatch defined by $\varepsilon=(a_t-a_s)\times 100/a_s$, where a_t and a_s are the lattice parameters of the bulk target and substrate, respectively, is calculated to be $\varepsilon\sim 0.51\%$. Thin films with thicknesses in the range of ~5–60 nm were deposited by on-axis dc magnetron sputtering on the single crystal STO substrates. Before deposition of the films, the chamber was cleaned by attaining a vacuum of up to $\sim 10^{-6}$ torr and then flushed twice by an Ar (80%) + O_2(20%) gas mixture. The substrate temperature was maintained at 800 °C at a dynamic pressure of 200 mtorr of Ar (80%)+O_2(20%). After deposition, the films were kept at 800 °C for half an hour at 1.0 torr gas pressure and then slowly cooled down to room temperature for more than 3 h. The films were then annealed in flowing oxygen at 750 °C.

Film thickness was measured for films that have step by

Downloaded 29 Apr 2009 to 202.141.140.34. Redistribution subject to AIP license or copyright; see http://jap.aip.org/jap/copyright.jsp

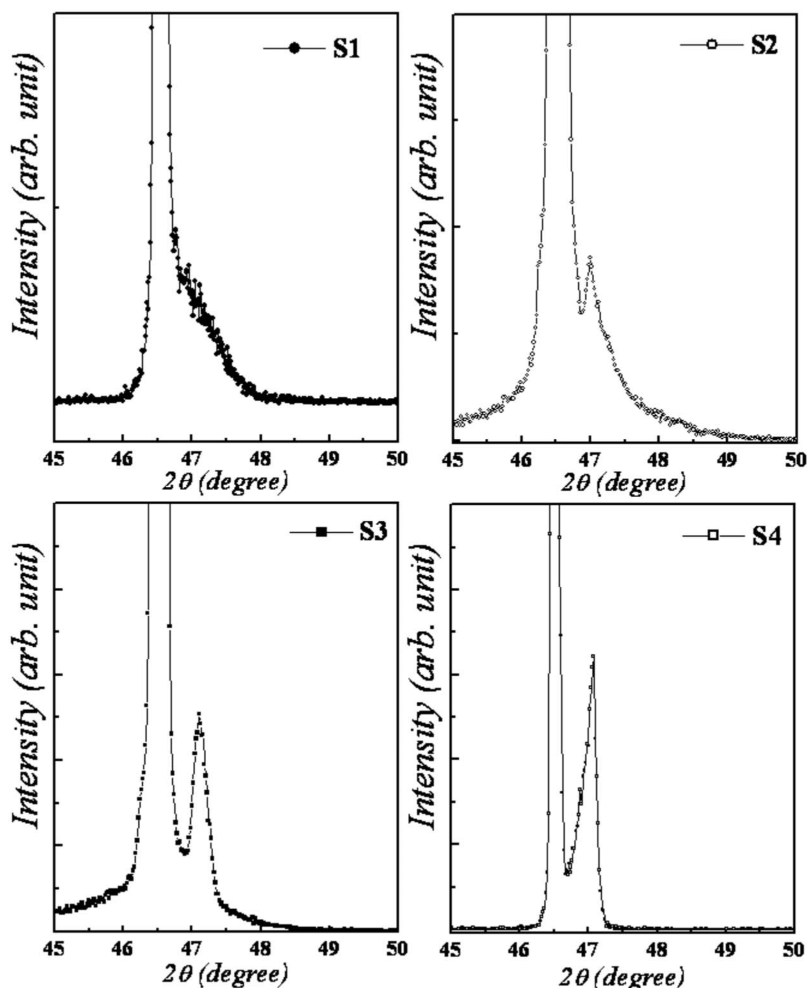

FIG. 1. Evolution of the (002) diffraction peak of $La_{0.88}Sr_{0.12}MnO_3$ thin films. In all panels, the higher intensity peak corresponds to the substrate.

a DEKTEK 6M surface profiler and atomic force microscope (AFM) in contact mode. The cationic composition was probed by energy dispersive x-ray analysis (EDAX). The structural characterization was carried out by employing XRD θ-2θ and rocking curve measurements. The surface morphology of all films was investigated by AFM in the contact mode. Magnetization measurements were performed in a superconducting quantum interference device magnetometer and magnetotransport measurements were performed in a physical properties measurement system (PPMS) (Quantum Design). For the sake of convenience, the films with thicknesses of 5, 17, 25, and 60 nm will hereafter be referred to as S1, S2, S3, and S4, respectively.

III. RESULTS AND DISCUSSION

EDAX analysis was carried out on the LS8812 film simultaneously deposited on ZrO_2 (in the case of films on STO, the presence of Sr makes it difficult to analyze the result). The average cationic composition was found to be La/Sr/Mn $\approx 0.89/0.12/0.99$, which is close to the nominal composition of the target. The very small spatial variation in the cationic composition suggests good chemical homogeneity of the films. XRD analysis employing θ-2θ scans and rocking curves showed that all the films are coherently grown and are epitaxial.[58] The evolution of the (002) diffraction maxima for all the films is shown in Figs. 1(a)–1(d). By using the XRD data, the out-of-plane lattice parameters of the films were extracted. For the 5 nm thin film on STO (S1), the out-of-plane lattice parameter was found to be very close to 3.905 Å, which gradually decreases to 3.87 Å for the 60 nm film. Clearly, the films with smaller thicknesses have larger out-of-plane lattice parameters and as the film thickness increases, the c lattice parameter is observed to decrease with increasing film thickness [as shown by the (00ℓ) diffraction peak shift to higher 2θ values] and approach the value of the c parameter of the bulk target. Thus, the out-of-plane lattice parameter of the film with the least thickness shows the maximum deviation from the corresponding bulk target value $c/2 \sim 3.87$ Å. The increased value of the out-of-plane lattice constant reflects the effect of biaxial compressive strain. In contrast to the out-of-plane c parameter, the in-plane lattice parameters are expected to acquire the substrate lattice constants, especially at lower thicknesses such as up to $L \sim 25$ nm (S3) in the present case. It has been shown that in films with very small thicknesses (such as S1, S2, and S3 in this study), the compressive strain in the a-b plane is dominant and, as a consequence, the in-plane lattice parameter of the film tends to acquire the same value as that of the substrate.[60,61] However, in thicker films, such as S4 ($L=60$ nm), there may be a strain gradient in the out-of-plane direction, resulting in partial relaxation of the strain. In general, a strained film possesses three distinct regions. The

Downloaded 29 Apr 2009 to 202.141.140.34. Redistribution subject to AIP license or copyright; see http://jap.aip.org/jap/copyright.jsp

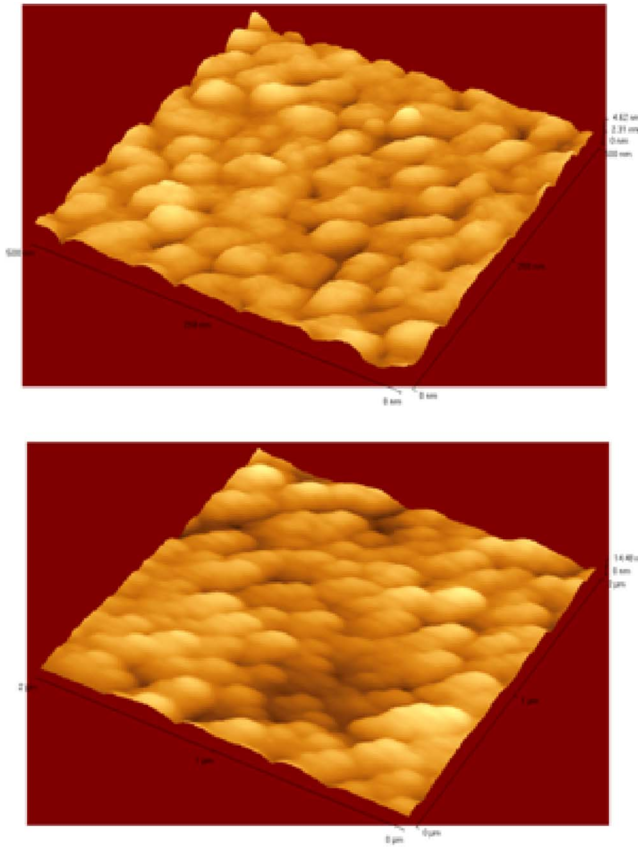

FIG. 2. (Color online) AFM pictures showing the surface morphologies of the 5 nm (top) and 60 nm (bottom) thin films. Better crystallinity is evident in the thicker film.

one in contact with the substrate is fully strained and, depending on the degree of lattice mismatch, it can extend up to several nanometers. The second region is characterized by a strain gradient, which diminishes as the film thickness increases. The third one is a strain-relaxed zone. The boundary between these regions may not be very sharp. At lower film thicknesses, only the fully strained state is expected. The gradual reduction in the out-of-plane c parameter with increasing film thickness, as revealed by XRD, suggests that there is indeed a strain relaxation. Hence, only the film with a thickness of ~ 5 nm may be fully strained and all the other films undergo partial strain relaxation. This relaxation, which is due to the presence of a strain gradient, will be spatially inhomogeneous, that is, the lower region close to the substrate will be more strained than the following layers. These layers may also be separated by an intrinsic interface containing a dislocation network.[17] The partial strain relaxation may result in the formation of other defects, such as cationic and oxygen vacancies and stacking faults, whose density depends on the degree of strain relaxation. The generation of such defects may enhance the JT distortion in the localized regions. The representative surface topographies of the 5 nm (S1) and 60 nm (S4) thin films are shown in Fig. 2. As revealed by the surface order, the films are coherently grown and even the 60 nm film has a highly ordered grain morphology. Evidently, the thicker film possesses better crystalline features. The average surface roughness was found to be less than 2 nm for all the films; it was observed to decrease with increasing film thickness. Coherently strained manganite films are known to develop morphological instability, resulting in a rough surface.[27]

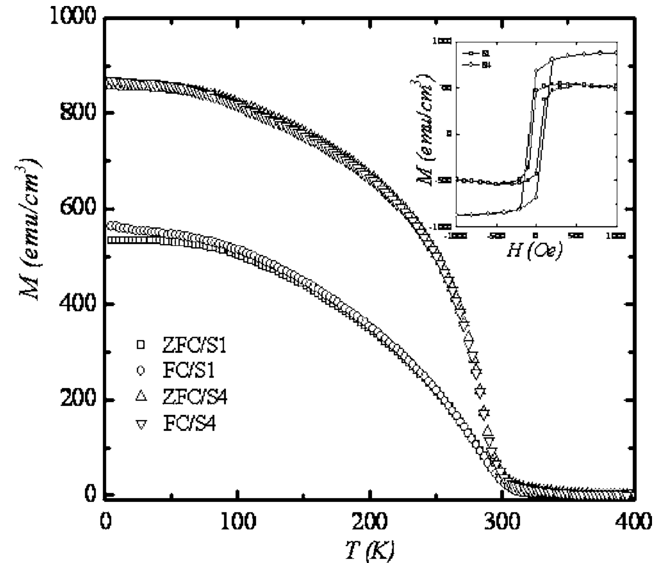

FIG. 3. Temperature dependence of dc magnetization (of 500 Oe) showing the PM-FM phase transition in the 5 nm (S1) and 60 nm (S4) thin films. The inset shows the M-H loop measured at 10 K.

Temperature dependent field cooled (FC) and zero FC (ZFC) dc magnetizations (M-T) were measured in the temperature range of 5–400 K at $H = 500$ Oe applied parallel to the film surface. The onset of the PM-FM transition was observed to be very close in films with thicknesses of up to 25 nm and it decreased only slightly for the 60 nm thick film. The representative M-T plots of S1 and S4 are shown in Fig. 3. The PM-FM transition temperature (T_C) was evaluated from the ZFC data and found to be 315 K for S1 and a small increase was observed as the film thickness increased to 25 nm ($T_C \sim 320$ K for S3). The 60 nm thick film showed a slightly reduced T_C, ~ 310 K. Thus, all the films show drastic enhancements in T_C as compared to the bulk sample (FM $T_C \sim 175$ K). The observed enhancement in T_C of films as compared to that of the bulk target can be explained as a consequence of the in-plane compressive strain.[60,61] The FC and ZFC data of ultrathin films ($L \leq 25$ nm) showed a small irreversibility, while no such feature was observed in the 60 nm thick film. The saturation magnetization (M_S) of the films was observed to increase as a function of film thickness and, in fact, for the thicker film (S4), $M_S \sim 850$ emu/cm^3, while $M_S \sim 525$ emu/cm^3 for the ultrathin S1 film, both at 5 K. In order to have further ideas about the nature of the FM phase, we measured the M-H loop of the films. The representative M-H data of the thinnest (S1) and thickest films (S4) taken at 10 K are plotted in the inset of Fig. 3. The coercivity (H_C) of the film with the smallest thickness (S1) is the smallest, $H_C \sim 55$ Oe. Coercivity as a function of film thickness gradually increases to $H_C \sim 92$ Oe for the ~ 60 nm film (S4). The nearly vertical and rectangular shaped M-H loop and small values of H_C are suggestive of the good quality of the films and indicate that these films possess near ideal FM characteristics. The T_C values are listed in Table I.

As mentioned above, the most striking feature of M-T is

Downloaded 29 Apr 2009 to 202.141.140.34. Redistribution subject to AIP license or copyright; see http://jap.aip.org/jap/copyright.jsp

TABLE I. Characteristic magnetic and transport parameters of $La_{0.88}Sr_{0.12}MnO_3$ thin films.

Film	Thickness (nm)	T_C (K)	T_{IM} (K)	MR (300 K)	TCR_{max}	E_A (meV)
S1	5	315	318	26	2.4	71
S2	17	316	321	36	3.2	62
S3	25	320	323	42	3.9	59
S4	60	310	313	47	5.5	80

the large enhancement in FM T_C as compared to the bulk sample used as the target (FM $T_C \sim 175$ K). The observed enhancement in T_C of the films as compared to that of the bulk target can be explained by taking the effect of compressive strain into account. As pointed out earlier, all the films are under in-plane compressive strain ($\varepsilon \sim 0.51\%$). It is well known that in low divalent-doped manganites such as $La_{0.88}Sr_{0.12}MnO_3$, the MnO_6 octahedrons are heavily distorted in the in-plane directions, and consequently, the JT effect dominates the DE, resulting in lower T_C values. Under compressive strain, MnO_6 octahedrons are compressed in the in-plane direction with simultaneous elongation in the out-of-plane direction, as shown by the enhanced *c* parameters of the films. This suppresses the JT distortion and causes a decrease in the in-plane Mn–O–Mn bond distance (d_{in}), and at the same time, the Mn–O–Mn bond angle (θ_{in}) approaches the ideal value, $\sim 180°$. Consequently, the in-plane transfer integral $t_x = t_y \sim (t_0/d_{in}^{3.5})\cos(\pi - \theta_{in})/2$ increases; hence, the DE is significantly enhanced, resulting in higher T_C. The slightly lower T_C of the 60 nm film (S4) can be attributed to the small relaxation of the strain due to increased film thickness.

Several other fine features are observed in the *M*-*T* data: (i) a small increase in T_C up to a film thickness of ~ 25 nm followed by a decrease for higher film thickness, (ii) a small irreversibility in the ZFC-FC curves that disappears at higher film thickness, and (iii) an increase in the saturation magnetization with film thickness. These features could be understood as follows: It is generally believed that in the case of the manganite thin films with a thickness less than a critical value, the magnetic and transport properties are dominated by the manganite-substrate interface.[17] The concept of the presence of magnetically dead layers has been proposed to account for the anomalous features in these films.[11,17,48] Two magnetically dead layers are present at both the film-substrate interface and the film surface, with a total thickness of around 25 nm whatever the film thickness ($20 \text{ nm} < L < 60$ nm) is. The magnetization rapidly falls off inside these interfaces due to spin canting, which induces loss of polarization.[17] This loss of polarization has been confirmed by spin-resolved photoemission spectroscopy on thick 130 nm LSMO films on STO.[60] The temperature dependence of the moment at the surface exhibits a markedly different behavior from that of the bulk magnetization. However, for the present films, the variation of T_C with thickness is rather small, and therefore, the concept of dead layer does not seem realistic. Further, the universality of the "dead layer" has been questioned by Ziese *et al.*[62] It was shown by them that the concept of dead layers is not always applicable and is too simple to capture the physics of manganites. The magnetic and transport properties of manganite films are dependent on the annealing conditions, that is, whether the films are annealed *ex situ* or *in situ*. It has also been theoretically shown that magnetic and transport properties depend on the degree of tetragonal distortion as well as on different strain states induced by the different annealing procedures.[60,62] It is also known that the breaking of the Mn^{4+}–O–Mn^{3+} network chain near the film-substrate interface causes induced phase separation.[24] This can cause a small deviation from the nominal Mn^{4+}/Mn^{3+} ratio in the vicinity of the interface. Furthermore, as ultrathin films are supposed to be under a large degree of substrate-induced strain, some chemical nonstoichiometry and interfacial oxygen vacancies are also possible. As the film thickness increases, these are stabilized. Thus, interface-induced phase separation leads to the creation of a magnetically disordered and chemically inhomogeneous state in the vicinity of the film-substrate interface, whose contribution is more prominent at lower film thicknesses. In the present study, the near ideal FM behavior as revealed by the *M*-*H* loop and the fact that the variation in T_C and magnetization up to film thickness $L \sim 25$ nm is rather small suggest that the concept of the dead layer may not be applied here. Hence, in compressively strained ultrathin films, the situation is intrinsically different, and in this case, the role of strain, which as discussed earlier modifies the two basic interactions, FM-DE and JT distortion, is expected to play the dominant role in fixing the magnetic and electrical transport properties. In this context, the role of magnetic disorder in the film-substrate interfacial region, which is caused by the loss of oxygen/oxygen vacancies and the nanometric level chemical nonstoichiometry, may be more relevant. In view of the magnetization measurements, we argue that in the present case, it is the presence of local inhomogeneities due to submicrometer/nanometer stoichiometry deviations that results in the small variations in magnetization and T_C up to $L \sim 25$ nm. The decrease in T_C by ~ 10 K for the 60 nm film, as discussed earlier, is attributed to the small degree of strain relaxation, as suggested by the reduced tetragonal distortions observed in the XRD data as well as the increase in the value of H_C. The small irreversibility in the ZFC-FC curves at lower film thicknesses can be attributed to the presence of some spin-clustered states having soft magnetic disorder caused by the interfacial phase separation. The contribution of this magnetically disordered state to total magnetization, however, becomes less important at higher film thicknesses. Thus, the most important factor that may cause a variation in physical properties, as a function of film thickness, is the presence of submicrometric/

Downloaded 29 Apr 2009 to 202.141.140.34. Redistribution subject to AIP license or copyright; see http://jap.aip.org/jap/copyright.jsp

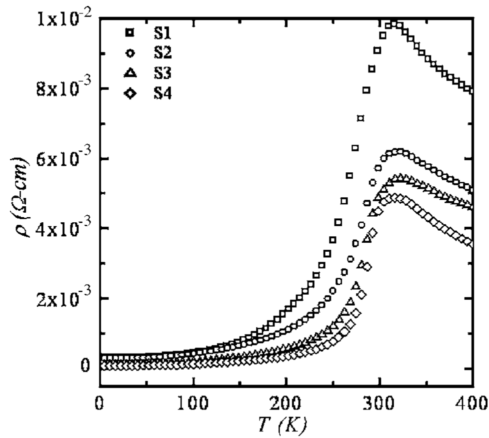

FIG. 4. Temperature dependence of zero field resistivities of the 5 nm (S1), 17 nm (S2), 25 nm (S3), and 60 nm (S4) thin $La_{0.88}Sr_{0.12}MnO_3$ films.

nanometric chemical inhomogeneities, resulting in interface-induced phase separation. Hence, in view of the small T_C enhancement at lower film thickness, this seems to be the more likely cause of small depression in T_C in the present case.

The resistivities of all films were measured by PPMS by employing the standard four contact technique between 400 and 5 K and at different magnetic fields of up to 70 kOe. The contacts were made of silver epoxy on copper pads sputtered on the films. The temperature dependence of resistivities measured in the zero magnetic field is plotted in Fig. 4. On lowering the temperature, all films showed IM-like transitions. The IM transition temperature (T_{IM}) characterized by the maximum in the ρ-T curve was found to be thickness dependent, the measured values being $T_{IM} \sim 318$, 321, 323, and 313 K, respectively, for S1, S2, S3, and S4. We would like to mention that among the several films grown under identical conditions and with the same thickness, a small variation in the T_{IM} (less than 2 K) as well as in the resistivity was observed. This can be attributed to the small spatial variation in the chemical stoichiometry. In all the films, T_{IM} was measured to be larger than the corresponding FM T_C. Like FM T_C, the T_{IM} values are much higher than that of the bulk target. With increasing film thickness, a gradual decrease in the resistivity was observed at all temperatures; e.g., at 5 K, the measured resistivities are 308, 285, 122, and 79.6 $\mu\Omega$ cm for S1, S2, S3, and S4, respectively. These values are slightly lower than those previously reported for such films[57] and are a check of the quality of the films. As it is evident from the ρ-T curves, with increasing film thickness, the decrease in the T_{IM} is accompanied by a sharpening of the transition and the thickest film (S4) has the smallest transition width. This trend is understood in terms of the magnetic characteristics of these films that were described earlier. As discussed earlier, it is observed that saturation magnetization increases with film thickness and that the thicker films (S4) have the highest value. The occurrence of magnetic disorder due to substrate-induced phase separation, which is more dominant at lower film thicknesses, would lead to increased scattering of carriers and, hence, larger resistivity. Thus this is the reason for the observed higher resistivity at lower thicknesses for our films. We would like to mention that at lower film thicknesses, the contribution of such inhomogeneities might further be enhanced under the influence of compressive strain. This may also result in additional scattering of the carriers and, hence, slightly higher resistivity in films with a smaller thickness.

To confirm that the observed variation in T_C/T_{IM} in epitaxial films on STO is caused by the biaxial strain and not by large stoichiometric deviation, we have simultaneously deposited and processed polycrystalline $La_{0.88}Sr_{0.12}MnO_3$ thin films on single crystal ZrO_2 (100) substrates and the measured T_C/T_{IM} is 180 K/193 K. The T_C is almost equal to that of the bulk ($\sim$175 K) but the T_{IM} is slightly higher and is due to some intrinsically better ordering in these thin films. However, for films deposited on ZrO_2, the resistivity is larger by almost 2 orders of magnitude than that of the films on STO. These results are being processed and will be separately reported. Thus, the observed enhancement in T_C/T_{IM} for the present $La_{0.88}Sr_{0.12}MnO_3$ ultrathin/thin films is due to the structural/microstructural modifications as a consequence of in-plane compressive strain.

As mentioned earlier, JT distortion of the oxygen octahedron can lead to the trapping of the charge carriers into a polaronic state, influencing the transport properties in the high temperature PM phase.[61] Hence, the temperature dependence of resistivity data in the PM regime is an important probe of the conduction mechanism. In manganite thin films, strong polaronic effects are expected at $T > T_{IM}$. We have investigated the resistivities of $La_{0.88}Sr_{0.12}MnO_3$ films in the high temperature regime in the framework of the Emin–Holstein approach of small polaron hopping in the adiabatic limit[63] given by the expression:

$$\rho(T) = ATe^{E_A/k_BT},$$

where

$$A = 2k_B/3ne^2a^2\nu.$$

Here, n is the polaron concentration, a is the site-to-site hopping distance, ν is the attempt frequency, and k_B is the Boltzmann constant. E_A is the activation energy, i.e., the height of the potential barrier, and $E_A = E_P/2 - t$. In general, the overlap integral t is so small that it could be neglected and then, $E_A \approx E_P/2$, or the polaron binding energy $E_P \approx 2E_A$.

In Fig. 5, $\ln(\rho/T)$ is plotted against the inverse of temperature $(1/T)$ and a linearity is observed at $T > T_{IM}$. The solid lines in the plot are linear fits to the experimental data. We calculated the activation energy E_A from the fitting parameter and observed a thickness dependence, which is depicted in Fig. 6, while Fig. 7 shows the variation in T_{IM} as a function of the activation energy. As seen in Fig. 6, the activation energy of the 5 nm (S1) ultrathin films is $E_A \approx 71$ meV. E_A decreases with increasing film thickness and, in fact, for the 17 nm (S2) and 25 nm (S3) thin films, $E_A \approx 61$ and 59 meV, respectively. A relatively stronger increase is observed in the activation energy at further higher film thickness and for the 60 nm film (S4), $E_A \approx 80$ meV. E_A are also shown in Table I. It is interesting to note that the valley in the E_A-L plot corresponds to the optimum T_{IM} values, while both the lower and higher thickness regimes possess

Downloaded 29 Apr 2009 to 202.141.140.34. Redistribution subject to AIP license or copyright; see http://jap.aip.org/jap/copyright.jsp

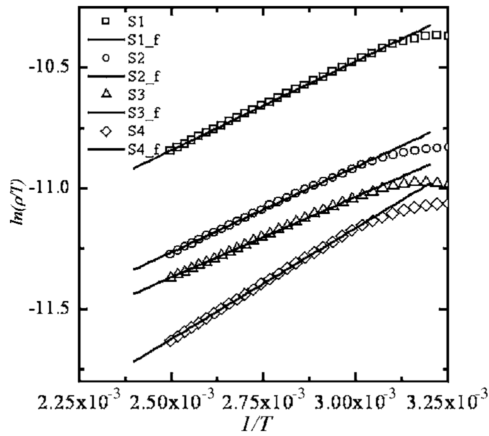

FIG. 5. T^{-1} vs $\ln(\rho/T)$ plots at $T > T_{IM}$ corresponding to the 5 nm (S1), 17 nm (S2), 25 nm (S3), and 60 nm (S4) thin $La_{0.88}Sr_{0.12}MnO_3$ films. The solid lines are fit to the measured data.

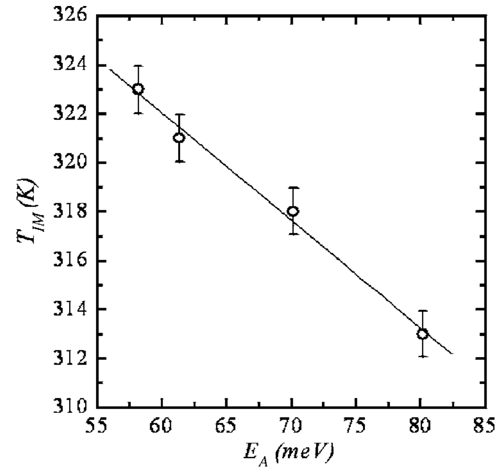

FIG. 7. Variation in IM transition temperature with activation energy.

lower T_{IM}. As detailed earlier, the 5 nm (S1) film has a T_{IM} ~ 318 K, which gradually increases to 323 K for S3 and decreases to ~ 313 K for S4. The variation of T_{IM} with E_A is plotted in Fig. 6 and within the experimental/measurement errors and sample-to-sample variation of results, the E_A-T_{IM} relation is nearly linear. The values of E_A of all the films are much smaller than that of the corresponding bulk. This suggests that JT has appreciably softened in thin films and this is brought about by the in-plane biaxial compressive strain. The variation in E_A as a function of film thickness can be understood in terms of the magnetic disorder caused by interfacial phase separation, localized chemical nonstoichiometry, and oxygen vacancies, as discussed earlier. This enhances the localization effects near the manganite-insulator (film-substrate) interface, resulting in the enhancement of the polaronic potential barrier and, hence, the increase in the activation energy. Such localization effect will be more dominant at a lower film thickness, resulting in enhanced resistivity and lower T_{IM} values for films with a lower thickness, such as S1 ($L = 5$ nm) in the present case.

The relatively strong increase in the activation energy of S4 ($L \sim 60$ nm) can be attributed to the small degree of strain relaxation. As seen in Fig. 6, E_A increases from ~ 59 meV ($T_{IM} \sim 323$ K) for the 25 nm thin film (S3) to ~ 80 meV ($T_{IM} \sim 313$ K) for the 60 nm film (S4). As discussed earlier, the 60 nm film has undergone partial relaxation due to increased thickness. Such strain relaxation resulting from increased film thickness is known to generate a variety of lattice defects, such as stacking faults, dislocation, and vacancies.[17] In the case of partial strain relaxation, these defects are expected to have a density gradient, that is, the density of such defects will vary as a function of the distance from the film-substrate interface. The presence of lattice defects enhances the JT distortion, and consequently, the carrier localization is strengthened, resulting in a larger value of the activation energy.

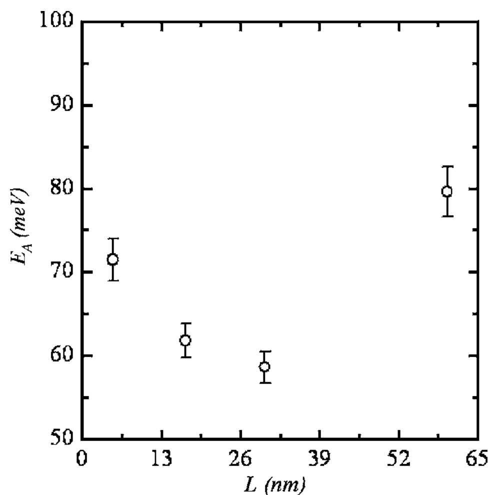

FIG. 6. Variation in the activation energy with film thickness.

Deep in the FM regime, the electrical transport is characterized by the presence of various inelastic interactions, such as electron-electron (e-e) scattering, electron-magnon (e-m) scattering, and disorder enhanced Coulomb interactions between carriers.[52,64] We have investigated the temperature dependent resistivity of all the films. As seen in Figs. 4 and 8, the ρ-T curve of all these films did not show any upturn and only the flattening of the resistivity was observed at $T < 30$ K. This again suggests that the present samples are of good quality. It is well known that the resistivity of manganites in the FM regime is quite well described by

$$\rho(T) = \rho_0 + \beta T^{\alpha},$$

where ρ_0 is the residual resistivity and the exponent α combines all possible interactions, such as e-e scattering ($\rho \sim T^2$) and e-m scattering ($\rho \sim T^{9/2}$). We fitted the low temperature resistivity data ($T \leq 150$ K) of all the films and a satisfactory fitting is obtained. However, small deviations are seen in the lower temperature regime for the ultrathin films ($L < 25$ nm). The values of the exponent α are found to be ~ 1.933, 2.334, 2.507, and 2.263. The deviation in the lower temperature regime ($T < 50$ K) has been generally accounted for by introducing an elastic scattering correction term of the $T^{1/2}$ type, which accounts for the disorder enhanced strong Coulomb interaction between the carriers.[64] Such a term is generally observed in a disordered metallic system and it changes sign as a function of disorder in the

Downloaded 29 Apr 2009 to 202.141.140.34. Redistribution subject to AIP license or copyright; see http://jap.aip.org/jap/copyright.jsp

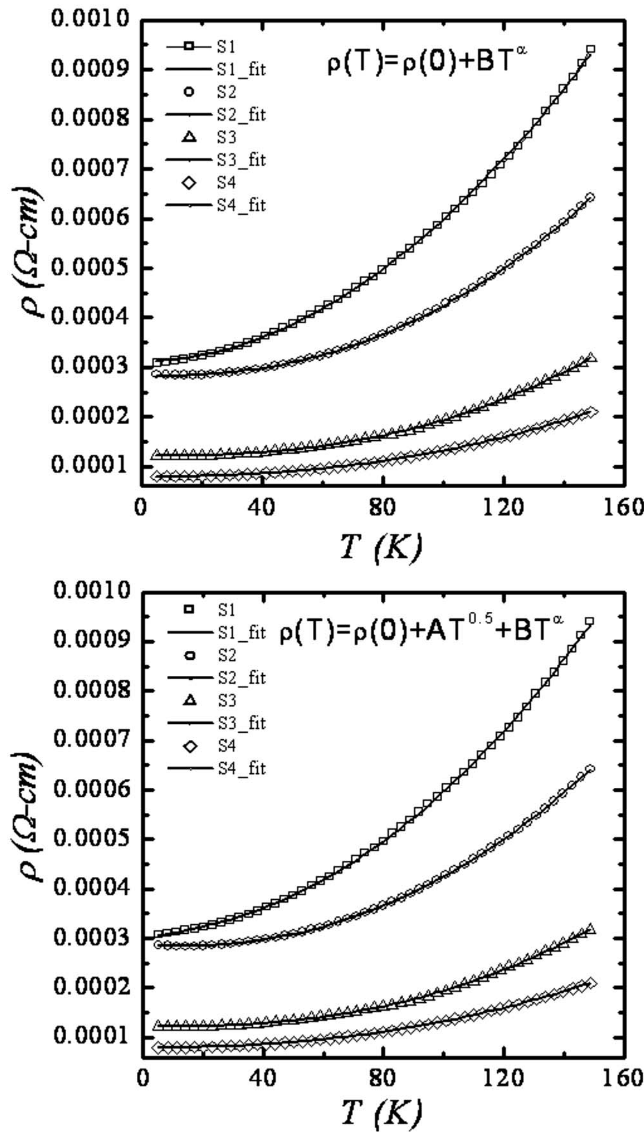

FIG. 8. Temperature dependence of resistivity in the low temperature regime (deep in the FM phase). The solid lines are fits of the equation shown in the inset to the observed data.

system. With this modification, the resistivity in the metallic FM regime is expressed by

$$\rho(T) = \rho_0 + AT^{1/2} + BT^{\alpha}.$$

By using this expression, the data of all the films were fitted and the values of the fitting parameters are shown in Table II. The observed and fitted data are plotted in Fig. 8. The value of the exponent α increases from 2.07 for S1 to 2.6 for S3 and then slightly decreases to 2.25 for S4. These values are in good agreement with those reported in literature.[52] This observed trend with $\alpha=2.07$ suggests that at $T<150$ K, the low temperature transport in the ultrathin film S1 (5 nm) is dominated by *e-e* scattering, with the contribution from other scattering mechanisms such as *e-m* ($\rho \sim T^{9/2}$) being rather small. As the film thickness slightly increases to 25 nm, the increase in the value of α to $\sim$2.6 suggests enhanced *e-m* contribution to the total resistivity. This is in agreement with the fact discussed earlier that the T_C/T_{IM} of these films maximize around a thickness of 15–25 nm. The contribution from *e-e* scattering in the 5 nm thin films can be explained in terms of the presence interface-induced phase separation and chemical nonstoichiometry, as described earlier. The second point to notice is that the Coulomb interaction term changes its sign with increased thickness and it becomes negative for all films with thicknesses greater than 5 nm. As has already been pointed out, the magnetic disordered region, which forms in the vicinity of the substrate, becomes less significant at higher film thicknesses. The decreased value of $\alpha \approx 2.25$ for S4 ($L=60$ nm) can be explained in terms of a small degree of strain relaxation that would result in the formation of lattice defects, such as stacking faults and dislocation, resulting in the eventual dilution of the FM phase. This, in turn, reduces the contribution from the *e-m* scattering.

Another property that is important from the application point of view is the TCR defined as $1/\rho(d\rho/dT)$. Most of the bolometric materials used (e.g., vanadium oxide) have a TCR $\sim$4% at around room temperature. However, the manganite films have been shown to exhibit a larger TCR but at a temperature much lower than room temperature.[65,66] In the present study, we have calculated the TCR of all the films and the data are plotted in Fig. 9. Films with thicknesses $L \geq 25$ nm exhibit significant TCR at around the room temperature. The values calculated from the resistivity data are (see also Table I) $\sim$4% and $\sim$5.5% for films with thicknesses of 25 nm (S3) and 60 nm (S4), respectively. These TCR values are indeed encouraging for IR detector device application.

The MR defined as $100 \times \Delta\rho/\rho(0)$, where $\Delta\rho = \rho(0) - \rho(H)$, was measured at different temperatures and magnetic fields. The temperature dependence of MR measured at low applied magnetic field $H=3$ kOe and at moderately high magnetic field $H=30$ kOe is plotted in Figs. 10(a) and 10(b). All the films possess significantly low field MR in the vicinity of room temperature and, in fact, this MR is much larger than that reported earlier for similar films.[60] The low field MR [Fig. 10(a)] is $\sim$6% at $H=3$ kOe for the ultrathin films (S1 and S2) and then gradually increases to $\sim$12% for the 60 nm (S4) film. A similar MR variation is observed at higher

TABLE II. Fitting parameters corresponding to the expression $\rho(T)=\rho_0+AT^{1/2}+BT^{\alpha}$.

Film	Thickness (nm)	α	ρ_0 (Ω cm)	A	B	R^2
S1	5	2.066	0.000 3	4.209×10^{-6}	1.908×10^{-8}	0.9998
S2	17	2.242	0.000 29	-1.667×10^{-6}	5.027×10^{-9}	0.9999
S3	25	2.594	0.000 12	-1.139×10^{-7}	5.027×10^{-10}	0.9997
S4	60	2.247	0.000 08	-1.058×10^{-7}	1.729×10^{-9}	0.9998

Downloaded 29 Apr 2009 to 202.141.140.34. Redistribution subject to AIP license or copyright; see http://jap.aip.org/jap/copyright.jsp

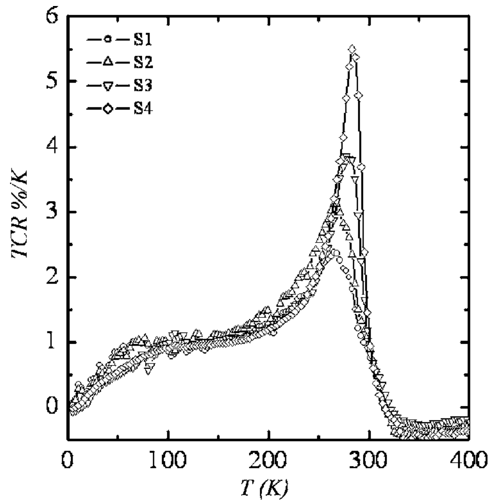

FIG. 9. Temperature dependence of TCR of the 5 nm (S1), 17 nm (S2), 25 nm (S3), and 60 nm (S4) thin $La_{0.88}Sr_{0.12}MnO_3$ films.

magnetic fields, e.g., the MR-T plot at $H=30$ kOe is shown in Fig. 10(b). The maximum observed in MR-T data shifts toward higher temperatures as the applied magnetic field increases. The 5 nm thin film has a peak in MR at ~ 285 K and $H=3$ kOe, which shifts to ~ 293 K at $H=30$ kOe. However, in all cases, this MR peak that is attributed to the FM-DE is observed at $T < T_{IM}$. MR gradually increases as a function of the applied magnetic field. At $H=30$ kOe, the 5 nm film shows a MR$\sim 28\%$ and significant enhancement is seen with an increase in film thickness. For the S4 film, which has the highest thickness in the present study, MR $\sim 50\%$ has been measured at $T \sim 295$ K ($H=30$ kOe). Thus, an enhancement in low as well as moderate field MRs is observed as a function of the increase in film thickness. The magnetic field dependence of MR for S1 and S4 measured at different temperatures (in PM as well as FM regimes) is plotted in Fig. 11. As seen in Fig. 10, the variation in MR in the vicinity of room temperature ($T < T_C$) is very sharp, while the observed variation is rather weak in the PM as well as deep in the FM regime. As mentioned earlier, the observed MR is much larger than those reported by Chen *et al.*[57] for similar films. At 300 K, Chen *et al.*[57] had observed MR $\sim 22\%$ at $H=30$ kOe, which is lower than MR$\sim 26\%$ for S1 (5 nm) and $\sim 47\%$ for S4 (60 nm) (see Table I). The room temperature MR in the present case is much higher than those recently reported by Siwach *et al.*[67] for Ag doped $La_{0.7}Ca_{0.3}MnO_3$ and Dho *et al.*[40] for $La_{0.7}Sr_{0.3}MnO_3$ thin films. We have mentioned these data as the T_C/T_{IM} of these Ag-LCMO films are nearly the same as those of the present LSMO thin films.

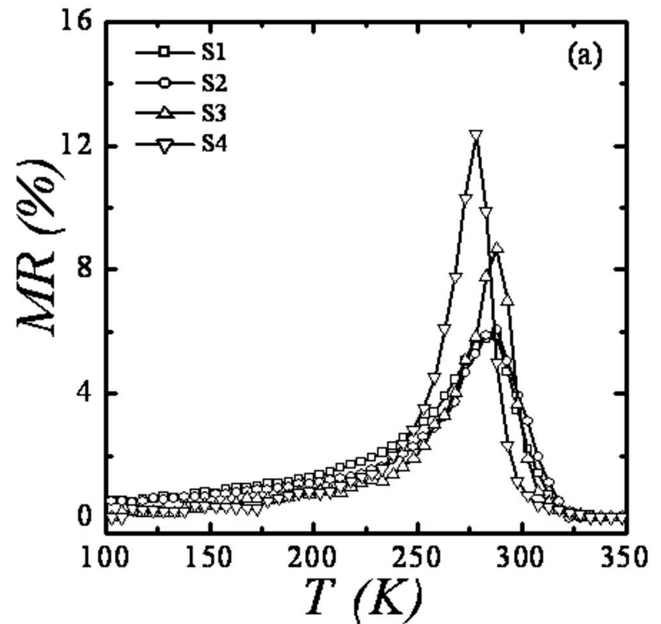

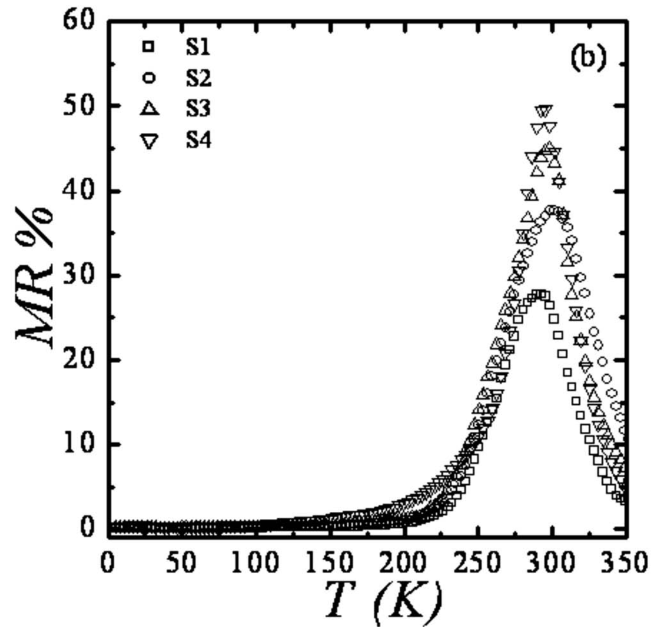

FIG. 10. Temperature dependence of low field ($H=3$ kOe) MR (a) and high field ($H=30$ kOe) MR (b) of the 5 nm (S1), 17 nm (S2), 25 nm (S3), and 60 nm (S4) thin $La_{0.88}Sr_{0.12}MnO_3$ films.

IV. CONCLUSIONS

Transport properties of thin films of lightly doped manganite $La_{0.88}Sr_{0.12}MnO_3$ deposited on STO substrate by on-axis dc magnetron sputtering have been studied. The films are observed to be under compressive strain and coherently grown. With increased film thickness, a gradual strain relaxation is seen. As compared to the bulk sample of the same composition, a large enhancement in T_C/T_{IM} is observed. The 25 nm thick film shows the highest T_C/T_{IM} ~ 320 K/323 K, which decreases for both the smaller and the larger film thicknesses. At lower film thicknesses, the decrease has been attributed to the presence of interface-induced disorder and chemical nonstoichiometry. At larger thicknesses of ~ 60 nm, the film undergoes partial strain relaxation and T_C/T_{IM} decrease by ~ 10 K. The activation energy calculated in the framework of the Emin–Holstein approach of small polaron hopping in the adiabatic limit is found to scale with film thickness and a minimum corresponding to the maximum T_C/T_{IM} is seen in the vicinity of 17–25 nm film thickness. Deep in the FM regime, the temperature dependence of resistivity is described well by $\rho(T)$

Downloaded 29 Apr 2009 to 202.141.140.34. Redistribution subject to AIP license or copyright; see http://jap.aip.org/jap/copyright.jsp

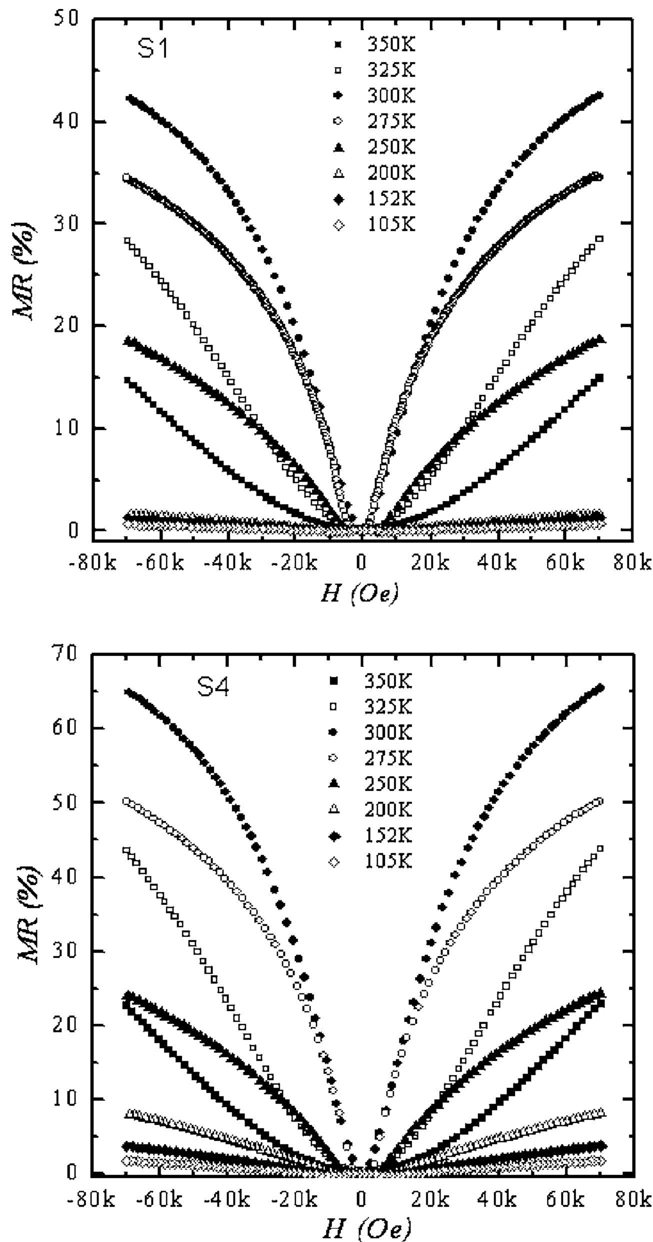

FIG. 11. Variation in MR of the 5 nm (S1) and 60 nm (S4) thin films with magnetic field.

$=\rho_0+AT^{1/2}+BT^{\alpha}$. All films show significant thickness dependent TCR ~ 5%/K and MR ~ 50% (both at low and high magnetic fields) just below T_C/T_{IM}.

ACKNOWLEDGMENTS

The authors are grateful to Professor Vikram Kumar for constant support and encouragement. Special thanks are due to Professor O. N. Srivastava (BHU, Varanasi) for stimulating discussions and support.

[1]R. von Helmolt, J. Wecker, B. Holzapfel, L. Schultz, and K. Samwer, Phys. Rev. Lett. **71**, 2331 (1993).
[2]S. Jin, T. H. Tiefel, M. McCormack, R. A. Fastnacht, R. Ramesh, and L. H. Chen, Science **264**, 413 (1994).
[3]P. Schiffer, A. P. Ramirez, W. Bao, and S.-W. Cheong, Phys. Rev. Lett. **75**, 3336 (1995).
[4]*Colossal Magnetoresistance Oxides*, edited by Y. Tokura (Gordon and Breach, New York, 2000).
[5]M. B. Salamon and M. Jaime, Rev. Mod. Phys. **73**, 583 (2001).
[6]J. M. D. Coey and M. Viret, Adv. Phys. **48**, 167 (1999).
[7]E. Dagotto, T. Hotta, and A. Moreo, Phys. Rep. **344**, 1 (2001).
[8]A. J. Millis, P. B. Littlewood, and B. I. Shraiman, Phys. Rev. Lett. **74**, 5144 (1995).
[9]A. J. Millis, B. I. Shraiman, and R. Mueller, Phys. Rev. Lett. **77**, 175 (1996).
[10]A. J. Millis, B. I. Shraiman, and R. Mueller, Nature (London) **392**, 147 (1998).
[11]J. Z. Sun, D. W. Abraham, R. A. Rao, and C. B. Eom, Appl. Phys. Lett. **74**, 3017 (1999).
[12]J. Li, C. K. Ong, J.-M. Liu, Q. Huang, and S. J. Wang, Appl. Phys. Lett. **76**, 1051 (2000).
[13]S. I. Khartsev, P. Johnsson, and A. M. Grishin, J. Appl. Phys. **87**, 2394 (2000).
[14]F. Tsui, M. C. Smoak, T. K. Nath, and C. B. Eom, Appl. Phys. Lett. **76**, 2421 (2000).
[15]F. S. Razavi, G. Gross, H.-U. Habermeier, O. Lebedev, S. Amelinckx, G. Van Tendeloo, and A. Vigliante, Appl. Phys. Lett. **76**, 155 (2000).
[16]W. Prellier, Ph. Lecoeur, and B. Mercey, J. Phys.: Condens. Matter **13**, R915 (2001).
[17]A.-M. Haghiri-Gosnet and J.-P. Renard, J. Phys. D **36**, R127 (2003).
[18]A. Biswas, M. Rajeswari, R. C. Srivastava, Y. H. Li, T. Venkatesan, R. L. Greene, and A. J. Millis, Phys. Rev. B **61**, 9665 (2000).
[19]J. Aarts, S. Freisem, R. Hendrikx, and H. W. Zandbergen, Appl. Phys. Lett. **72**, 2975 (1998).
[20]M. Izumi, Y. Konishi, T. Nishihara, S. Hayashi, M. Shinohara, M. Kawasaki, and Y. Tokura, Appl. Phys. Lett. **73**, 2497 (1998).
[21]J. N. Eckstein, I. Bozovic, J. O'Donnell, M. Onellion, and M. S. Rzchowski, Appl. Phys. Lett. **69**, 1312 (1996).
[22]K. Dörr, J. M. de Teresa, K.-H. Müller, D. Eckert, T. Walter, E. Vlakhov, K. Nenkov, and L. Schultz, J. Phys.: Condens. Matter **12**, 7099 (2000).
[23]F. S. Razavi, G. Gross, H.-U. Habermeier, O. Lebedev, S. Amelinckx, G. Van Tendeloo, and A. Vigliante, Appl. Phys. Lett. **76**, 155 (2000).
[24]M. Bibes, L. Balcells, S. Valencia, and J. Fontcuberta, Phys. Rev. Lett. **87**, 067210 (2001).
[25]J. Zhang, H. Tanaka, T. Kanki, J. H. Choi, and T. Kawai, Phys. Rev. B **64**, 184404 (2001).
[26]T. Kanki, H. Tanaka, and T. Kawai, Phys. Rev. B **64**, 224418 (2001).
[27]M. Ziese, H. C. Semmelhack, and K. H. Han, Phys. Rev. B **68**, 134444 (2003).
[28]S. Valencia, L. I. Balcells, J. Fontcuberta, and B. Martinez, Appl. Phys. Lett. **82**, 4531 (2003).
[29]M. Paranjape, A. K. Raychaudhuri, N. D. Mathur, and M. G. Blamire, Phys. Rev. B **67**, 214415 (2003).
[30]J. Klein, J. B. Philipp, G. Carbone, A. Vigliante, L. Alff, and R. Gross, Phys. Rev. B **66**, 052414 (2002).
[31]J. Klein, J. B. Philipp, D. Reisinger, M. Opel, A. Marx, A. Erb, L. Alff, and R. Gross, J. Appl. Phys. **93**, 7373 (2003).
[32]S. Jacob, T. Roch, F. S. Razavi, G. M. Gross, and H.-U. Habermeier, J. Appl. Phys. **91**, 2232 (2002).
[33]K. H. Ahn, T. Lookman, and A. R. Bishop, Nature (London) **428**, 401 (2004).
[34]Z. Q. Yang, R. Hendrikx, J. Aarts, Y. L. Qin, and H. W. Zandbergen, Phys. Rev. B **70**, 174111 (2004).
[35]F. Giesen, B. Damaschke, V. Moshnyaga, K. Samwer, and G. A. Müller, Phys. Rev. B **69**, 014421 (2004).
[36]A. Palanisami, M. B. Weissman, and N. D. Mathur, Phys. Rev. B **71**, 014423 (2005).
[37]A. Urushibara, Y. Moritomo, T. Arima, A. Asamitsu, G. Kido, and Y. Tokura, Phys. Rev. B **51**, 14103 (1995).
[38]H. Kawano, R. Kajimoto, M. Kubota, and H. Yoshizawa, Phys. Rev. B **53**, R14709 (1996).
[39]K. Steenbeck, T. Habisreuther, C. Dubourdieu, and J. P. Sénateur, Appl. Phys. Lett. **80**, 3361 (2002).
[40]J. Dho, Y. N. Kim, Y. S. Hwang, J. C. Kim, and N. H. Hur, Appl. Phys. Lett. **82**, 1434 (2003).
[41]Y. P. Lee, S. Y. Park, V. G. Prokhorov, V. A. Komashko, and V. L. Svetchnikov, Appl. Phys. Lett. **83**, 777 (2003).
[42]D. Talbayev, H. Zhao, G. Lüpke, J. Chen, and Q. Li, Appl. Phys. Lett. **86**, 182501 (2005).
[43]T. F. Zhou, G. Li, X. G. Li, S. W. Jin, and W. B. Wu, Appl. Phys. Lett. **90**, 042512 (2007).
[44]P. Dey, T. K. Nath, and A. Taraphder, Appl. Phys. Lett. **91**, 012511 (2007).

Downloaded 29 Apr 2009 to 202.141.140.34. Redistribution subject to AIP license or copyright; see http://jap.aip.org/jap/copyright.jsp

[45]F. Tsui, M. C. Smoak, T. K. Nath, and C. B. Eom, Appl. Phys. Lett. **76**, 2421 (2000).
[46]Z.-H. Wang, G. Cristiani, H.-U. Habermeier, Z.-R. Zhang, and B.-S. Han, J. Appl. Phys. **94**, 5417 (2003).
[47]J. Dho, N. H. Hur, I. S. Kim, and Y. K. Park, J. Appl. Phys. **94**, 7670 (2003).
[48]M. Angeloni, G. Balestrino, N. G. Boggio, P. G. Medaglia, P. Orgiani, and A. Tebano, J. Appl. Phys. **96**, 6387 (2004).
[49]H. L. Liu, M. X. Kuo, J. L. Her, K. S. Lu, S. M. Weng, S. L. Cheng, and J. G. Lin, J. Appl. Phys. **97**, 113528 (2005).
[50]H. L. Liu, K. S. Lu, M. X. Kuo, L. Uba, S. Uba, L. M. Wang, and H.-T. Jeng, J. Appl. Phys. **99**, 043908 (2006).
[51]V. Bhosle, J. T. Prater, and J. Narayan, J. Appl. Phys. **102**, 013527 (2007).
[52]S. Mercone, C. A. Perroni, V. Cataudella, C. Adamo, M. Angeloni, C. Aruta, G. De Filippis, F. Miletto, A. Oropallo, P. Perna, A. Yu. Petrov, U. Scotti di Uccio, and L. Maritato, Phys. Rev. B **71**, 064415 (2005).
[53]B. Dabrowski, X. Xiong, Z. Bukowski, R. Dybzinski, P. W. Klamut, J. E. Siewenie, O. Chmaissem, J. Shaffer, C. W. Kimball, J. D. Jorgensen, and S. Short, Phys. Rev. B **60**, 7006 (1999).
[54]Y. Moritomo, A. Asamitsu, and Y. Tokura, Phys. Rev. B **51**, 16491 (1995).
[55]F. S. Razavi, G. V. Sudhakar Rao, H. Jalili, and H.-U. Habermeier, Appl. Phys. Lett. **88**, 174103 (2006).
[56]X. J. Chen, S. Soltan, H. Zhang, and H.-U. Habermeier, Phys. Rev. B **65**, 174402 (2002).
[57]X. J. Chen, H.-U. Habermeier, H. Zhang, G. Gu, M. Varela, J. Santamaria, and C. C. Almasan, Phys. Rev. B **72**, 104403 (2005).
[58]R. Prasad, M. P. Singh, P. K. Siwach, W. Prellier, and H. K. Singh, Solid State Commun. **142**, 445 (2007).
[59]P. K. Siwach, U. K. Goutam, P. Srivastava, H. K. Singh, R. S. Tiwari, and O. N. Srivastava, J. Phys. D **39**, 14 (2006).
[60]Z. Fang, I. V. Solovyev, and K. Terakura, Phys. Rev. Lett. **84**, 3169 (2000).
[61]M. Ziese and C. Srinitiwarawong, Phys. Rev. B **58**, 11519 (1998).
[62]M. Ziese, H. C. Semmelhack, K. H. Han, S. P. Sena, and H. J. Blythe, J. Appl. Phys. **91**, 9930 (2002).
[63]D. Emin and T. Holstein, Ann. Phys. (Paris) **53**, 439 (1969).
[64]D. Kumar, J. Sankar, J. Narayan, R. K. Singh, and A. K. Majumdar, Phys. Rev. B **65**, 094407 (2002).
[65]A. Goyal, M. Rajeswari, R. Shreekala, S. E. Lofland, S. M. Bhagat, T. Boettcher, C. Kwon, R. Ramesh, and T. Venkatesan, Appl. Phys. Lett. **71**, 2536 (1997).
[66]R. J. Choudhary, A. S. Ogale, S. R. Shinde, S. Hullavarad, S.B. Ogale, and T. Venkatesan, Appl. Phys. Lett. **84**, 3846 (2004).
[67]P. K. Siwach, V. P. S. Awana, S. Balamurugan, E. Takayama-Muromachi, H. Kishan, O. N. Srivastava, R. Prasad, and H. K. Singh, J. Appl. Phys. **101**, 073912 (2007).

Downloaded 29 Apr 2009 to 202.141.140.34. Redistribution subject to AIP license or copyright; see http://jap.aip.org/jap/copyright.jsp